Topological states in a two-dimensional metal alloy in Si surface: BiAg/Si(111)-4 × 4 surface

Xiaoming Zhang,[1,2,3] Bin Cui,[2,3] Mingwen Zhao,[3,*] and Feng Liu[2,4,†]

[1]*Institute for Advanced Study, Tsinghua University, Beijing 100084, China*
[2]*Department of Materials Science and Engineering, University of Utah, Salt Lake City, Utah 84112, USA*
[3]*School of Physics and State Key Laboratory of Crystal Materials, Shandong University, Jinan, Shandong 250100, China*
[4]*Collaborative Innovation Center of Quantum Matter, Beijing 100084, China*

A bridging topological state with a conventional semiconductor platform offers an attractive route towards future spintronics and quantum device applications. Here, based on first-principles and tight-binding calculations, we demonstrate the existence of topological states hosted by a two-dimensional (2D) metal alloy in a Si surface, the BiAg/Si(111)-4 × 4 surface, which has already been synthesized experimentally. It exhibits a topological insulating state with an energy gap of 71 meV ($\sim$819 K) above the Fermi level and a topological metallic state with *quasiquantized* conductance below the Fermi level. The underlying mechanism leading to the formation of such nontrivial states is revealed by analysis of the "charge-transfer" and "orbital-filtering" effect of the Si substrate. A minimal effective tight-binding model is employed to reveal the formation mechanism of the topological states. Our finding opens opportunities to detect topological states and measure its quantized conductance in a large family of 2D surface metal alloys, which have been or are to be grown on semiconductor substrates.

I. INTRODUCTION

With the feature of quantized spin Hall conductance (SHC) [1,2], the topological states of two-dimensional (2D) materials were extensively studied due to their fundamental interest and potential applications ranging from spintronics to quantum computation. While the prediction of topological edge states has been well developed [3–5], to date only two quantum well systems, HgTe/CdTe and InAs/GaSb [6,7], have been confirmed that have nontrivial edge states of quantized conductivity but too small a band gap.

Earlier studies have shown topological edge states of Bi on nonsemiconducting substrates, such as Bi(111)/Bi_2Te_3 [8–10], Bi(110)/graphite [11], and Bi(111)/Sb [12], but there is unwanted hybridization between the overlayer topological states and substrate trivial states. To overcome this problem, an interesting idea was proposed to take advantage of the so-called "orbital-filtering" effect of the substrate [13], so that the topological state can be induced by depositing metal, such as a Bi honeycomb lattice on the semiconductor surface, such as Si [13], SiC [14], or Ge [15] surface, without hybridization. The resulting large nontrivial gap and the conductive edge state have been experimentally confirmed on SiC surface recently [14]. The topological edge state has also been theoretically predicted and experimentally confirmed in a 2D superconductor overlayer in FeSe/$SrTiO_3$(001) [16], which offers an intriguing platform to study topological superconducting states. However, all these experiments are based on spectroscopy measurements without showing the quantized edge conductivity. The challenge is largely due to a lack of experimental samples with a large single-surface domain of a perfect metal overlayer. Therefore, the search for 2D topological states continues; especially, a bridging topological state with a conventional semiconductor platform to realize topological states at high temperature is of great interest.

Taking a known experimental example of BiAg alloy on a Si(111)-4 × 4 surface [see Fig. 1(a)] [17], here we show that the BiAg/Si(111)-4 × 4 surface has four topologically nontrivial bands stemming from the p_{xy} orbitals of the Bi atoms, which are well decoupled from other states; this is attributed to the charge-transfer and orbital-filtering effect of the silicon substrate. A minimal effective tight-binding (TB) model on a honeycomb lattice is employed to explain the existence of these topological states. Specifically, the topological insulating (TI) state above the Fermi level exhibits a SHC of $-2e/4\pi$ within the nontrivial gap of $\sim$71 meV, while that of the topological metallic (TM) state below the Fermi level is mixed with trivial metallic states but still shows a finite width of quantized conductance plateau up to $\sim$50 meV. Our findings suggest that the common 2D surface metal alloys on semiconductors provide a viable family of candidate materials for searching large gap topological states with robust quantized conductance plateau.

II. METHOD AND COMPUTATIONAL DETAILS

The electronic and topological properties of the BiAg/Si(111)-4 × 4 surface were calculated using the Vienna *ab initio* simulation package (VASP) [18,19] and WANNIER90 [20] within the framework of density functional theory (DFT). The generalized gradient approximation in the Perdew-Burke-Ernzerhof form [21] and projector-augmented-wave potentials with an energy cutoff of 500 eV [22] were, respectively, used for describing
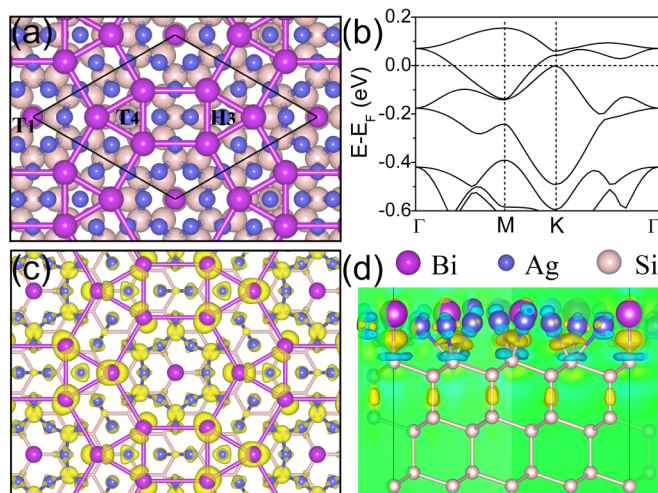
FIG. 1. (a) Schematic representation of the BiAg/Si(111)-4 × 4 surface with the unit cell indicated by a rhombus. Only the Si atoms of the top bilayer were plotted for clarity. Bi@T_4 and Bi@H_3 are bonded together to highlight the ruby lattice pattern. (b) Band structure of the BiAg/Si(111)-4 × 4 surface without considering SOC. The Fermi level is set to zero. (c) The charge density distribution of the four isolated bands at all the K points sampled in the BZ. (d) Illustration of charge transfer between the BiAg alloy and the silicon substrate, which is calculated by subtracting the charge density of the freestanding BiAg alloy and the surface-exposed silicon substrate from the total charge density of the BiAg/Si(111)-4 × 4 surface. The yellow (blue) isosurfaces indicate the increase (decrease) of electronic density.

the electron-electron and electron-ion interactions. Structural optimizations were performed using a conjugate gradient method on a 3 × 3 × 1 Monkhorst-Pack sampling until the remanent force on each atom was less than 0.01 eV/Å, while a dense Gamma-centered sampling (6×6×1) is employed for charge density calculations and establishing the maximally localized Wannier functions (MLWFs).

III. RESULTS AND DISCUSSION

The top view of the BiAg/Si(111)-4 × 4 surface is displayed in Fig. 1(a); it is prepared by depositing about one monolayer of Ag onto the mixed Si(111) α-$\sqrt{3}$ × $\sqrt{3}$/β-$\sqrt{3}$ × $\sqrt{3}$-Bi surface followed by annealing at ∼250 °C [17]. One unit cell of the BiAg/Si(111)-4 × 4 surface has seven bismuth atoms and 20 silver atoms. Besides a single Bi atom located at the T_1 site, other Bi atoms form two triangles located over the T_4 and H_3 sites. Hence we name the three types of bismuth as Bi@T_1, Bi@T_4, and Bi@H_3, whose positions can be seen more clearly from Fig. S1 in the Supplemental Material [23]. The Bi@T_4 and Bi@H_3 construct a perfect ruby lattice pattern [24], which is highlighted in Fig. 1(a). The outmost Si atoms of the top bilayer can also be distinguished through the number of their nearest Bi or Ag atoms.

Figure 1(b) shows the calculated electronic band structures of the BiAg/Si(111)-4 × 4 surface without considering spin-orbit coupling (SOC), and one clearly sees four bands near the Fermi level which are well decoupled from the other bands. In addition to the quadratic points emerging at the Γ point,
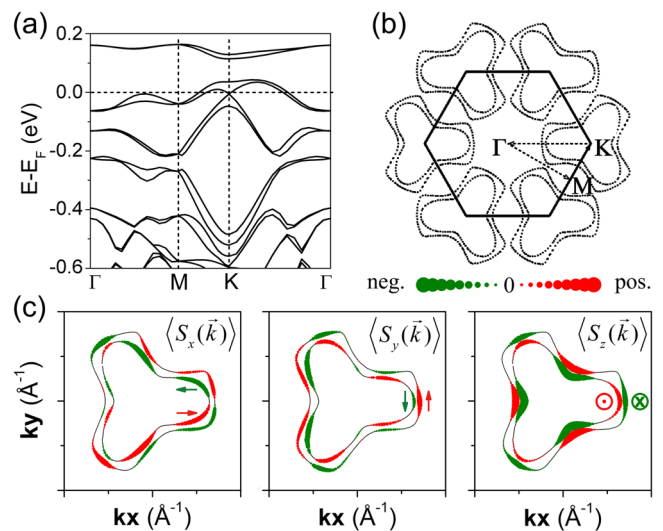

FIG. 2. (a) SOC included band structure and (b) Fermi surface contour of the BiAg/Si(111)-4 × 4 surface. The Fermi surface contour formed by the Dirac cone near the Fermi level was very small and hence not plotted. (c) The spin polarization $\langle s_x(\vec{k})\rangle$, $\langle s_y(\vec{k})\rangle$, $\langle s_z(\vec{k})\rangle$ at the Fermi surface contour. Red (green) color represents parallel (antiparallel) to the projected direction of x, y, and z, respectively.

band crossing takes place along the path from the Γ to the M point, while no degeneracy (Dirac point) exists at the K point. By plotting the charge density distribution of the four isolated bands in Fig. 1(c), we conclude that these bands stem mainly from the p_{xy} orbitals of Bi@T_4 and Bi@H_3, while the contributions from the other atoms are almost negligible except the p_z orbitals of the Si atoms with the three nearest Ag atoms. Notably, the tiny different charge density isosurfaces of Bi@T_4 and Bi@H_3 imply that they are not exactly equivalent due to the substrate effect, which breaks the inversion symmetry so that no Dirac point forms between the two middle bands at the K point. The absence of any electronic states from the Ag atoms around the Fermi level can be attributed to the significant charge transfer from the BiAg alloy to the silicon substrate, as shown in Fig. 1(d). Furthermore, the increased electronic density at the interface indicates bond formation, particularly the formation of Bi-Si bonds that have pushed the p_z orbital of Bi atoms away from the Fermi level. This in turn enables the isolation of p_{xy} bands near the Fermi level to be well decoupled from other electronic states. Such mechanism is similar to a Bi honeycomb lattice on a semiconductor substrate [13]. To confirm this, we performed a computational experiment of calculating the band structure of isolated BiAg alloy without substrate (as a hypothetical model system), as shown in Fig. S2 [23]. In addition to the states arising from the Bi p_{xy} orbitals, one can clearly see the metallic states dominated by Ag atoms and the p_z orbital of Bi atoms around the Fermi level, which were removed by the orbital-filtering and "charge-transfer" effect of the Si substrate.

Taking the SOC into account, the degeneracy at quadratic points and band crossing points is lifted, with significant spin splitting in eight bands, as shown in Fig. 2(a). We notice a large SOC energy gap of ∼71 meV is opened up above the Fermi level, and new degenerate points (Dirac cone) are formed at

the six corners of the first Brillouin zone (BZ). Here we should point out that the Dirac cone is not protected by symmetry since a weaker SOC strength will destroy it (Fig. S3) [23]. Actually, the gap closing at the K point between the two middle bands is the critical point of phase transition that we will show below. The Fermi surface contour is plotted in Fig. 2(b), which illustrates highly anisotropic properties, consistent with the anisotropic dispersions of the four isolated bands near the Fermi level.

Spin polarizations in the x, y, and z directions [$\langle s_x(\vec{k})\rangle$, $\langle s_y(\vec{k})\rangle$, $\langle s_z(\vec{k})\rangle$], defined as $\langle s_\alpha(\vec{k})\rangle = \langle\varphi(\vec{k})|\sigma_\alpha|\varphi(\vec{k})\rangle$, ($\alpha = x, y, z$) [25], in the Fermi surface contour were calculated to show the spin texture in Fig. 2(c). In addition to the nonzero spin polarization in the x and y directions, $\langle s_z(\vec{k})\rangle$ has the same order of magnitude as $\langle s_{x/y}(\vec{k})\rangle$ and hence cannot be neglected. Based on the Hamiltonian of extrinsic SOC $\hat{H}_{\mathrm{SOC}} \propto \boldsymbol{\sigma} \cdot (\boldsymbol{\nabla} V \times \hat{\mathbf{p}})$, it is easy to show that the nonzero $\langle s_{x/y}(\vec{k})\rangle$ components stem from the out-of-plane potential energy gradient due to the breaking of inversion symmetry in a surface, while the out-of-plane spin polarization is induced by an in-plane potential energy gradient contributed mainly by the surface BiAg alloy (Fig. S4 [23]), in which the surrounding Ag atoms play a significant role. Considering the nonzero $\langle s_z(\vec{k})\rangle$ is always accompanied by anisotropic Fermi surface contours without a perfect circular shape [26], one can understand that the surrounding Ag atoms have modified the dispersions of the four bands by affecting the electron hopping between the p_{xy} orbitals of Bi@T_4 and Bi@H_3.

In order to further reveal the above mechanism, we construct a minimal effective TB model by placing both the p_x and p_y orbitals on a honeycomb lattice [Fig. 3(a)], where the second-neighbor hopping parameters, t^1 and γ, can be regarded as the electron hopping induced by the surrounding Ag atoms. The Hamiltonian is written as $H = H_0 + H_{\mathrm{SOC}}$ and details can be found in the Supplemental Material [23]. Diagonalizing the Hamiltonian of H_0 in reciprocal space, we obtain four bands plotted in Fig. 3(b), which show exactly the same features as the isolated four bands of BiAg/Si(111)-4 × 4 surface shown in Fig. 1(b), including the quadratic point, bands crossing point, and the absence of the Dirac point resulting from the different on-site energies attained by the orbitals in the different sublattices. When considering the intrinsic SOC [27,28], all the degenerate points are lifted and new Dirac points emerge at the six corners of the first BZ [Fig. 3(c)], similar to the above DFT results. Then we examine the band evolution with respect to the decrease of the electron hopping parameters (t^1, γ), to simulate the effect of decreasing the perturbations of the surrounding Ag atoms, as plotted in Figs. S5(a)–S5(c) [23]. One can clearly see that the four bands [Fig. 3(c)] gradually evolve into the well-known four topological bands composed of two Dirac bands sandwiched by two flat bands [Fig. 3(d)] [27]. This indicates that the perturbations of the surrounding Ag atoms only distort the shape (i.e., dispersion) of Dirac and flat bands but without closing or reopening any gap, so that the topology of all four bands remains intact. Thus the fours bands in Figs. 3(c) and 3(d) share the same topological property.

Next we investigate the topological properties of the BiAg/Si(111)-4 × 4 surface. We first confirm the existence of nontrivial topological edge states, which can be directly compared with the experimental results of spectroscopic tech-
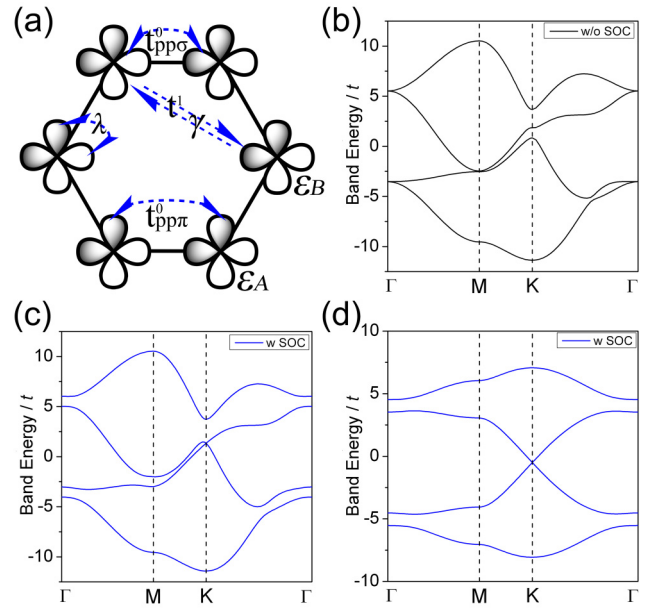

FIG. 3. (a) Schematic of the p_{xy} orbitals TB model on a honeycomb lattice with the illustrations of neighbor hopping ($t_{pp\sigma}^0$, $t_{pp\pi}^0$) and second-neighbor hopping (t^1, γ). λ indicates the intrinsic SOC strength between the p_x and p_y orbitals. ε_A and ε_B are the on-site energy of the p_{xy} orbitals on different sublattice. (b,c) Band dispersions of the TB model (b) without and (c) with considering SOC. (d) The typical four topological bands evolved from the bands in figure (c) by removing the perturbations of surrounding Ag atoms.

niques [8–12,14,16]. The plane-averaged charge density along the z axis (Fig. S6 [23]) indicates the formation of 2D electron gas at the surface of the silicon substrate. Hence a recursive strategy is employed to construct the edge Green's function of the *semi-infinite* lattice from MLWFs [29], which were established by defining the p_{xy} orbitals on a honeycomb lattice to generate the initial guess for the unitary transformations. The Wannier-interpolated band structure is plotted in Fig. 4(a), which shows good agreement with the DFT bands [Fig. 2(a)]. The local density of states (LDOS) calculated from the edge Green's function is plotted in Fig. 4(b). One can clearly see two topological Dirac-like edge states respectively located at the energy window above and below the Fermi level, indicating that some finite amount of n doping or p doping can turn the system into either a TI or a TM. Next, we calculated the topological invariants to confirm the nontriviality of bands. By means of time-reversal polarization [30], we track the *largest gap* between the adjusted Wannier charge centers (WCCs) [31]. Figure 4(c) shows the determination of the Z_2 invariant with k_x treated as the pumping parameter running from 0 to π for an effective one-dimensional (1D) system. Kramers pairs form at $k_x = 0$ and π, but not elsewhere. Each blue dot represents the center of the largest gap between the adjusted WCCs. We see that the gap center jumps down over one WCC, which is odd. Thus the Z_2 index is 1, indicating the nontriviality.

Knowing the existence of topological states in a BiAg/Si(111)-4 × 4 surface, we further studied the SHC as obtained from the so-called spin Chern number calculation [32] to characterize the robustness of the transverse electrical transport property against temperature perturbations and trivial
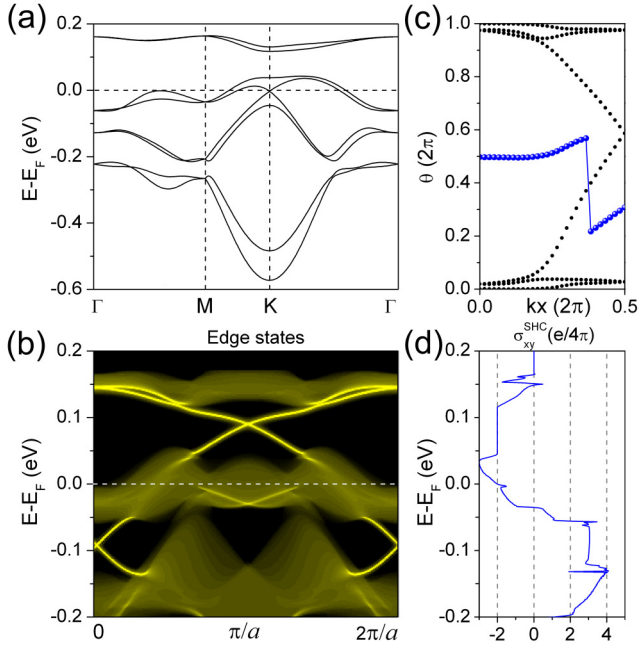
FIG. 4. (a) The Wannier-interpolated band structure and (b) the semi-infinite edge states of the BiAg/Si(111)-4 × 4 surface with considering SOC. (c) Evolutions of WCCs versus k_x at the nontrivial gap above the Fermi level. Blue dots mark the center of the largest gap between adjusted WCCs. (d) The SHC as a function of electron filling.
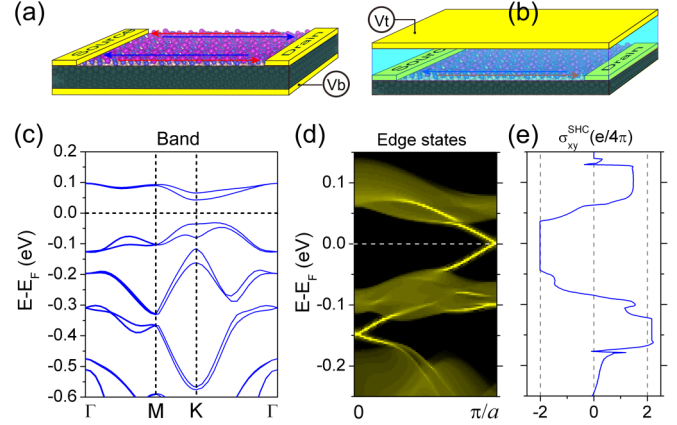

FIG. 5. A schematic illustration of the experimental setup for realizing electron/hole doping by using (a) back gate (V_b) and (b) top gate (V_t) voltage. (c) Band structure, (d) semi-infinite edge states, and (e) calculated SHC of the BiAg/Si(111)-4 × 4 surface with Bi@T_1 being substituted by a Te atom. The Fermi level is set at the middle of the nontrivial gap.

metallic states, where a wide and stable quantized conductance plateau is desired. The definition of the spin Chern number is $C_s = \frac{1}{2\pi} \int_{\text{BZ}} d^2\vec{k} \sum_n f_{nk} \Omega_n^s(\vec{k})$ with the Fermi distribution function of f_{nk} and the spin Berry curvature of $\Omega_n^s(\vec{k}) = -2\text{Im} \sum_{m \neq n} \frac{\langle \psi_{nk}|j_x|\psi_{mk}\rangle \langle \psi_{mk}|v_y|\psi_{nk}\rangle}{(\varepsilon_{mk}-\varepsilon_{nk})^2}$; here ψ_{nk} is the eigenstate of eigenvalue ε_{nk} of band n, j_x is the spin-velocity operator defined as $(s_z v_x + v_x s_z)/2$, and s_z and $v_{x/y}$ are the spin operator and the velocity operator, respectively. Figure 4(d) shows the calculated SHC ($\sigma_{xy}^{\text{SHC}} = 2C_s \frac{e}{4\pi}$) as a function of the electron filling. The quantized value of $-2e/4\pi$ within the SOC gap above the Fermi level indicates the characteristic transport property of the quantum spin Hall (QSH) insulator, which is robust against finite perturbations because of a large nontrivial bulk gap (∼71 meV) that cannot be easily closed. Moreover, because the nontrivial Dirac edge states are well isolated from other trivial metallic states below the Fermi level [see Fig. 4(b)], the TM state also shows a quasiquantized feature with a width of conductance plateau up to ∼50 meV, indicating a certain degree of robustness against trivial metallic states [33,34].

The robust plateau of the SHC indicates a promising perspective for experimentally measuring the quantized conductivity of nontrivial edge states in a BiAg/Si(111)-4 × 4 surface, similar to that observed in the HgTe/CdTe and InAs/GaSb quantum well [6,7], but with a large energy gap. The well-developed doping technology based on semiconducting substrates, such as gating that can realize carrier doping with the concentration ranging from 10^{12} to 10^{14} cm^{-2} [35–37], can

be taken advantage of to include a system with nonintrinsic topological states.

Specifically, for transport experiments and future device application, one needs to dope one electron/hole per unit cell (doping concentration: 4.83×10^{13} cm^{-2}) to move the Fermi level up/down to the energy range of nontrivial states. Given that the BiAg/Si(111)-4 × 4 surface is composed of a 2D monolayer of BiAg alloy and semiconducting substrate, standard gating technology should be easily applicable to dope this system. It is feasible for both the back gate (V_b) and top gate (V_t) to reach the desired doping level of ∼10^{13} cm^{-2}, as shown in Figs. 5(a) and 5(b). This same method has been successfully used to measure the conductance of QSH states in HgTe/CdTe quantum wells, in which the carrier concentration was tuned from n to p type through applying an external gate voltage [6]. Additionally, we would like to discuss another possible doping strategy, that is, substituting the atom of the host material itself, which has been found effective for Bi$_2$Te$_3$ [38], Bi$_2$Se$_3$ [39], and Bi$_2$Te$_2$Se [40]. Phosphorus/boron substituting of a Si atom of substrate provides a feasible method of realizing doping because they are well-established industrial technologies [41–43]. Moreover, we believe that substituting Bi@T_1 with group VI/IV elements can also realize electron/hole doping without disturbing the topological property of the BiAg/Si(111)-4 × 4 surface. The feasibility of such method is based on previous orbital analysis. As we discussed above, the p_{xy} orbitals of Bi@T_4 and Bi@H_3 contribute mainly to the four nontrivial bands near the Fermi level, while Bi@T_1 and other atoms have little contribution. Taking tellurium (Te) as an example, our calculations show that a Te atom prefers to substitute Bi@T_1 rather than Bi@T_4 and Bi@H_3 by about 91.8 and 69.6 meV/unit cell, respectively. The atomic structure of the BiAg/Si(111)-4 × 4 surface with Bi@T_1 being substituted by a Te atom is shown in Fig. S7 [23]. The Te atom plays the role of electron doping and moves the Fermi level up to the energy gap of the TI state successfully [Fig. 5(c)], while maintaining the nontrivial topology as characterized by the Dirac-like edge

states [Fig. 5(d)]. SHC calculation [Fig. 5(e)] also confirms the robust transport property of the topological state against atomic substitution.

We note that the system we explore here represents a 2D metal alloy of BiAg on a Si(111)-4 × 4 surface, which is different from that of growing a metal overlayer such as Bi on a Au-covered Si surface, such as a Au/Si(111)-$\sqrt{3} \times \sqrt{3}$ surface [44], in several important aspects. In our system, Bi atoms sit in a ruby lattice, while in that system it is a hexagonal or trigonal lattice. Consequently, the resulting topological band structures and underlying formation mechanism are also different.

IV. CONCLUSION

We demonstrate from first-principles calculations that the already-synthesized BiAg/Si(111)-4 × 4 surface has robust topological nontrivial edge states rising from the p_{xy} orbitals of Bi, which are well decoupled from the other electronic states due to charge transfer and bond formation between the BiAg alloy and the Si substrate. The topological property is confirmed by calculations of edge states, WCCs, and spin Chern number, and analyzed with a minimal effective TB model.

Electron doping will transform a BiAg/Si(111)-4 × 4 surface into a 2D TI with a nontrivial gap of 71 meV, corresponding to a temperature up to 819 K for a QSH effect. Hole doping converts the BiAg/Si(111)-4 × 4 surface into a 2D TM, where a finite-quantized conductance plateau of ∼50 meV is still observable because of the limited interference from the trivial metallic states. Therefore, the BiAg/Si(111)-4 × 4 surface provides a promising material platform for detecting nontrivial topological edge states and investigating its exotic transport properties, and we await future experiments to confirm our theoretical predictions.

[1] C. L. Kane and E. J. Mele, Phys. Rev. Lett. **95**, 226801 (2005).

[2] B. A. Bernevig, T. L. Hughes, and S.-C. Zhang, Science **314**, 1757 (2006).

[3] M. Z. Hasan and C. L. Kane, Rev. Mod. Phys. **82**, 3045 (2010).

[4] X.-L. Qi and S.-C. Zhang, Rev. Mod. Phys. **83**, 1057 (2011).

[5] Y. F. Ren, Z. H. Qiao, and Q. Niu, Rep. Prog. Phys. **79**, 066501 (2016).

[6] M. König, S. Wiedmann, C. Brüne, A. Roth, H. Buhmann, L. W. Molenkamp, X.-L. Qi, and S.-C. Zhang, Science **318**, 766 (2007).

[7] I. Knez, R.-R. Du, and G. Sullivan, Phys. Rev. Lett. **107**, 136603 (2011).

[8] F. Yang, L. Miao, Z. F. Wang, M.-Y. Yao, F. Zhu, Y. R. Song, M.-X. Wang, J.-P. Xu, A. V. Fedorov, Z. Sun, G. B. Zhang, C. Liu, F. Liu, D. Qian, C. L. Gao, and J.-F. Jia, Phys. Rev. Lett. **109**, 016801 (2012).

[9] Z. F. Wang, M.-Y. Yao, W. Ming, L. Miao, F. Zhu, C. Liu, C. L. Gao, D. Qian, J.-F. Jia, and F. Liu, Nat. Commun. **4**, 1384 (2013).

[10] T. Hirahara, G. Bihlmayer, Y. Sakamoto, M. Yamada, H. Miyazaki, S.-I. Kimura, S. Blugel, and S. Hasegawa, Phys. Rev. Lett. **107**, 166801 (2011).

[11] Y. Lu, W. Xu, M. Zeng, G. Yao, L. Shen, M. Yang, Z. Luo, F. Pan, K. Wu, T. Das, P. He, J. Jiang, J. Martin, Y. P. Feng, H. Lin, and X.-S. Wang, Nano Lett. **15**, 80 (2015).

[12] G. Bian, Z. Wang, X. X. Wang, C. Xu, S. Xu, T. Miller, M. Z. Hasan, F. Liu, and T. C. Chiang, ACS Nano **10**, 3859 (2016).

[13] M. Zhou, W. Ming, Z. Liu, Z. Wang, P. Li, and F. Liu, Proc. Natl. Acad. Sci. USA **111**, 14378 (2014).

[14] F. Reis, G. Li, L. Dudy, M. Bauernfeind, S. Glass, W. Hanke, R. Thomale, J. Schäfer, and R. Claessen, Science **357**, 287 (2017).

[15] P. Li, M. Zhou, L. Z. Zhang, Y. H. Guo, and F. Liu, Nanotechnology **27**, 095703 (2016).

[16] Z. F. Wang, H. Zhang, D. Liu, C. Liu, C. Tang, C. Song, Y. Zhong, J. Peng, F. Li, C. Nie, L. Wang, X. J. Zhou, X. Ma, Q. K. Xue, and Feng Liu, Nat. Mater. **15**, 968 (2016).

[17] N. V. Denisov, E. N. Chukurov, Y. V. Luniakov, O. A. Utas, S. G. Azatyan, A. A. Yakovlev, A. V. Zotov, and A. A. Saranin, Surf. Sci. **623**, 17 (2014).

[18] G. Kresse and J. Furthmüller, Phys. Rev. B **54**, 11169 (1996).

[19] G. Kresse and J. Hafner, Phys. Rev. B **48**, 13115 (1993).

[20] A. A. Mostofi, J. R. Yates, Y.-S. Lee, I. Souza, D. Vanderbilt, and N. Marzari, Comput. Phys. Commun. **178**, 685 (2008).

[21] J. P. Perdew, K. Burke, and M. Ernzerhof, Phys. Rev. Lett. **77**, 3865 (1996).

[22] G. Kresse and D. Joubert, Phys. Rev. B **59**, 1758 (1999).

[23] See Supplemental Material at http://link.aps.org/supplemental/10.1103/PhysRevB.97.085422 for the illustration of position for Bi@T_1, Bi@T_4, and Bi@H_3, projected band structures of the freestanding BiAg alloy, the variation of band structure of the BiAg/Si(111)-4 × 4 surface when manually modifying SOC strength, details of our minimal effective TB model, the plane-averaged electrostatic potential energy and charge density, and the atomic structure of the BiAg/Si(111)-4 × 4 surface with Bi@T_1 being substituted by a Te atom.

[24] X. Hu, M. Kargarian, and G. A. Fiete, Phys. Rev. B **84**, 155116 (2011).

[25] W. Ming, Z. F. Wang, M. Zhou, M. Yoon, and F. Liu, Nano Lett. **16**, 404 (2016).

[26] C. R. Ast, J. Henk, A. Ernst, L. Moreschini, M. C. Falub, D. Pacilé, P. Bruno, K. Kern, and M. Grioni, Phys. Rev. Lett. **98**, 186807 (2007).

[27] C. Wu, Phys. Rev. Lett. **101**, 186807 (2008).

[28] Z. Liu, Z.-F. Wang, J.-W. Mei, Y.-S. Wu, and F. Liu, Phys. Rev. Lett. **110**, 106804 (2013).

[29] M. P. L. Sancho, J. M. L. Sancho, J. M. L. Sancho, and J. Rubio, J. Phys. F: Met. Phys. **15**, 851 (1985).

[30] L. Fu and C. L. Kane, Phys. Rev. B **74**, 195312 (2006).

[31] A. A. Soluyanov and D. Vanderbilt, Phys. Rev. B **83**, 235401 (2011).

[32] D. N. Sheng, Z. Y. Weng, L. Sheng, and F. D. M. Haldane, Phys. Rev. Lett. **97**, 036808 (2006).

[33] A. Junck, K. W. Kim, D. L. Bergman, T. Pereg-Barnea, and G. Refael, Phys. Rev. B **87**, 235114 (2013).

[34] Y.-Y. Zhang, M. Shen, X.-T. An, Q.-F. Sun, X.-C. Xie, K. Chang, and S.-S. Li, Phys. Rev. B **90**, 054205 (2014).

[35] K. Ueno, S. Nakamura, H. Shimotani, A. Ohtomo, N. Kimura, T. Nojima, H. Aoki, Y. Iwasa, and M. Kawasaki, Nat. Mater. **7**, 855 (2008).

[36] K. S. Novoselov, A. K. Geim, S. V. Morozov, D. Jiang, Y. Zhang, S. V. Dubonos, I. V. Grigorieva, and A. A. Firsov, Science **306**, 666 (2004).

[37] A. Das, S. Pisana, B. Chakraborty, S. Piscanec, S. K. Saha, U. V. Waghmare, K. S. Novoselov, H. R. Krishnamurthy, A. K. Geim, A. C. Ferrari, and A. K. Sood, Nat. Nanotechnol. **3**, 210 (2008).

[38] Y. L. Chen, J. G. Analytis, J.-H. Chu, Z. K. Liu, S.-K. Mo, X. L. Qi, H. J. Zhang, D. H. Lu, X. Dai, Z. Fang, S. C. Zhang, I. R. Fisher, Z. Hussain, and Z.-X. Shen, Science **325**, 178 (2009).

[39] Y. S. Hor, A. Richardella, P. Roushan, Y. Xia, J. G. Checkelsky, A. Yazdani, M. Z. Hasan, N. P. Ong, and R. J. Cava, Phys. Rev. B **79**, 195208 (2009).

[40] Z. Ren, A. A. Taskin, S. Sasaki, K. Segawa, and Y. Ando, Phys. Rev. B **85**, 155301 (2012).

[41] E. Baek, T. Rim, J. Schütt, C.-K. Baek, K. Kim, L. Baraban, and G. Cuniberti, Nano Lett. **17**, 6727 (2017).

[42] E. A. Ekimov, V. A. Sidorov, E. D. Bauer, N. N. Mel'nik, N. J. Curro, J. D. Thompson, and S. M. Stishov, Nature **428**, 542 (2004).

[43] B. Slomski, G. Landolt, G. Bihlmayer, J. Osterwalder, and J. Hugo Dil, Sci. Rep. **3**, 1963 (2013).

[44] B. Huang, K.-H. Jin, H. L. Zhuang, L. Zhang, and F. Liu, Phys. Rev. B **93**, 115117 (2016).